Electrochemistry Communications 24 (2012) 116–119

Contents lists available at SciVerse ScienceDirect

Electrochemistry Communications

journal homepage: www.elsevier.com/locate/elecom

Sodium iron pyrophosphate: A novel 3.0 V iron-based cathode for sodium-ion batteries

Prabeer Barpanda [a], Tian Ye [a], Shin-ichi Nishimura [a,b], Sai-Cheong Chung [a], Yuki Yamada [a,b], Masashi Okubo [a,c], Haoshen Zhou [a,c], Atsuo Yamada [a,b,*]

[a] Department of Chemical System Engineering, School of Engineering, The University of Tokyo, 5-604, 7-3-1 Hongo, Bunkyo-Ku, Tokyo 113-8656, Japan
[b] Unit of Elements Strategy Initiative for Catalysts & Batteries, ESICB, Kyoto University, Kyoto 615-8510, Japan
[c] Energy Technology Research Institute, National Institute of Advanced Industrial Science and Technology (AIST), Umezeno 1-1-1, Tsukuba 305-8568, Japan

ARTICLE INFO

Article history:
Received 19 August 2012
Received in revised form 31 August 2012
Accepted 31 August 2012
Available online 10 September 2012

Keywords:
Na-ion batteries
Cathode
Pyrophosphate
$Na_2FeP_2O_7$

ABSTRACT

Extending the pyrophosphate chemistry for rechargeable Na-ion batteries, here we report the synthesis and electrochemical characterization of $Na_2FeP_2O_7$, a novel Fe-based cathode material for sodium batteries. Prepared by conventional solid-state as well as solution-combustion synthesis (at 600 °C), the $Na_2FeP_2O_7$ adopts a triclinic structure (space group: *P*-1) with three-dimensional channels running along [100], [−110] and [01-1] directions. With no further optimization, the as-synthesized $Na_2FeP_2O_7$ cathode was found to be electrochemically active, delivering a reversible capacity of 82 mAh·g^{-1} with the Fe^{3+}/Fe^{2+} redox potential centered around 3 V (vs. Na/Na$^+$). With its theoretical capacity of ~100 mAh·g^{-1} and potential high rate-capability, $Na_2FeP_2O_7$ forms a promising novel cathode material, with the distinction of being the first ever pyrophosphate-class of cathode for sodium-ion batteries.

1. Introduction

Towards the goal of realizing sustainable and greener energy scenario, economic and efficient energy-storage and (remote) supply form a key challenge. In this context, rechargeable Li-ion batteries have become a frontrunner device empowering small-scale portable electronics to large-scale (hybrid) electric vehicles [1]. In parallel to the massive effort on lithium batteries, recently sodium-ion batteries have attracted renewed interest owing to the abundance of sodium resources [2]. In this quest, a variety of oxides (e.g. Na_xCoO_2, $NaCrO_2$, $NaVO_2$, $Na_x(Fe_{1/2}Mn_{1/2})O_2$) and polyanionic cathodes (e.g. $NaFePO_4$, $Na_3V_2(PO_4)_3$, $NaVPO_4F$, Na_2FePO_4F, $NaFeSO_4F$) has been reported [3–10]. In the search for new sodium cathodes, a family of several polyanionic framework materials can be explored. With our recent success in Li metal pyrophosphate ($Li_2MP_2O_7$) cathodes [11,12], we extended the pyrophosphate chemistry for possible discovery of potential sodium-based cathode materials. Surprisingly, there has been no report on a sodium metal pyrophosphate ($Na_{2-x}MP_2O_7$) class of cathode, although it has been extensively investigated by crystallographers for the past four decades [13]. Recently, a mixed-polyanionic cathode [$Na_4Fe_3(PO_4)_2(P_2O_7)$] having both PO_4 and P_2O_7 units has been reported [14]. Embarking on the mission to find a $Na_{2-x}MP_2O_7$ pyrophosphate cathode, our natural priority was to prepare $Na_2FeP_2O_7$, a previously unknown compound. It can be easily prepared by conventional one-step solid-state synthesis. Exploring the rich pyrophosphate chemistry, we hereby report $Na_2FeP_2O_7$ as a new cathode compound for sodium-ion batteries with promising electrochemical properties involving a 3.0 V Fe^{3+}/Fe^{2+} redox activity.

2. Material and methods

The target compound ($Na_2FeP_2O_7$) was prepared by conventional one-step solid-state route. A 2:1 molar mixture of NaH_2PO_4 (Wako, 99%) and $FeC_2O_4.2H_2O$ (Junsei, 99%) was intimately mixed by planetary ball-milling for 2 h (400 rpm) in acetone. For milling, Cr-hardened stainless steel (Cr-SS) milling media and container were used. After evaporating the acetone in vacuum, the precursor mixture was ground and calcined at 600 °C for 10–12 h in a tubular furnace (with steady Ar flow) to obtain the final product. Alternately, $Na_2FeP_2O_7$ was made by a splash combustion synthesis using stoichiometric amount of NaH_2PO_4 and $Fe^{III}(NO_3)_3{\cdot}9H_2O$ (Wako, 99%) along with citric acid ($C_6H_8O_7$, Wako, 98%) combustion agent, involving the final calcination step at 600 °C for 6 h. The detailed explanation of this splash combustion synthesis has been reported elsewhere [15]. The desodiated $Na_{2-x}FeP_2O_7$ samples were obtained from the solid-state synthesized compound via chemical oxidation using NO_xBF_4 (x = 1, 2) (Alfa Aesor, 96%) oxidizing agents dissolved in acetonitrile solvent (Wako, H_2O level < 5 ppm).

* Corresponding author at: Department of Chemical System Engineering, School of Engineering, The University of Tokyo, 5-604, 7-3-1 Hongo, Bunkyo-Ku, Tokyo 113-8656, Japan. Tel.: +81 3 5841 7295; fax: +81 3 5841 7488.
E-mail addresses: prabeer@chemsys.t.u-tokyo.ac.jp (P. Barpanda), yamada@chemsys.t.u-tokyo.ac.jp (A. Yamada).

1388-2481/$ – see front matter © 2012 Elsevier B.V. All rights reserved.
http://dx.doi.org/10.1016/j.elecom.2012.08.028

The solution was stirred overnight (with steady argon bubbling) and the final products were filtered and dried at 60 °C.

Powder X-ray diffraction pattern was collected in the 2θ range of 10–90° (with the step size of 0.02°) by using a Rigaku RINT-TTR III powder diffractometer (operating at 300 mA, 50 kV), equipped with a Cu-Kα radiation source ($\lambda_1 = 1.54056$ Å, $\lambda_2 = 1.54439$ Å). Rietveld refinement was performed using TOPAS-Academic Ver. 4.1 [16]. The Mössbauer spectra were measured with a Topologic System Inc. spectrometer with a ^{57}Co γ-ray source, calibrated with α-Fe as standard. The model fitting was performed with MossWinn 3.0 software [17]. SEM imaging was conducted on powder samples mounted on conducting carbon paste by a Hitachi S-4800 FE-SEM unit operating at 5 kV.

For electrochemical measurements, the working electrode was formulated by ball milling 75 wt.% $Na_2FeP_2O_7$ active material made by solution-combustion synthesis, 20 wt.% acetylene black (AB) and 5 wt.% polytetrafluoro-ethylene (PTFE) binder. This working electrode tape was pressed on an Al mesh working as the current collector, with an average cathode loading of 3 mg/cm^2. Beaker-type three-electrode cells were assembled inside an Ar-filled glove box by taking the cathode film as the working electrode and Na metal foils acting as counter and reference electrodes. These beaker cells were filled with 1 M $NaClO_4$ dissolved in propylene carbonate (PC) acting as electrolyte with no additives. Galvanostatic charge–discharge cycling was conducted in the voltage range of 2.0–4.0 V at different rates (from C/20 to 10 C) (at 25 °C).

3. Results and discussion

Independent of the synthesis routes, the $Na_2FeP_2O_7$ product was found to assume a triclinic framework with *P*-1 symmetry, isostructural to the triclinic polymorph of $Na_2CoP_2O_7$ as reported by Erragh et al. [18]. Interestingly, $Na_2CoP_2O_7$ stabilizes into three polymorphs: orthorhombic ($P2_1cn$), tetragonal ($P4_2/mnm$) and triclinic (*P*-1) phases, the orthorhombic phase being the most stable one [18,19]. Contrary to our speculation, for $Na_2FeP_2O_7$, the triclinic phase was always obtained independent of the synthesis conditions. The X-ray diffraction pattern of solid-state prepared $Na_2FeP_2O_7$ sample is illustrated in Fig. 1, where Rietveld refinement shows majority (90%) of the desired product formation along with traces of impurities like $Na_4P_2O_7$ (7%), maricite $NaFePO_4$ (1.5%) and $Na_4Fe_3(PO_4)_2(P_2O_7)$ (1.4%). The former two impurity phases are thermodynamically quite stable and electrochemically inactive. The $Na_2FeP_2O_7$ assumes a triclinic (space group: *P*-1) structure with lattice parameters: $a = 6.43382(16)$ Å, $b = 9.4158(3)$ Å, $c = 11.0180(3)$ Å, $\alpha = 64.4086(15)°$, $\beta = 85.4794(19)°$, $\gamma = 72.8073(17)°$ and $Vol = 574.16(3)$ Å^3. Similar results were obtained for the solution synthesized sample. It is built from FeO_6 octahedral and PO_4 tetrahedral building blocks, connected in a staggered fashion thus creating large tunnels along the [011] direction accommodating the Na atoms. The crystal structure contains corner-sharing Fe_2O_{11} dimers (i.e. FeO_6–FeO_6), which are interconnected by the characteristic P_2O_7 diphosphate units, both by corner-sharing and edge-sharing fashion. The constituent Na ions occupy four distinct crystallographic sites (Fig. 1, inset). A series of isostructural non-stoichiometric $Na_{2-2x}Fe_{1+x}P_2O_7$ compositions can be formed similar to previously-reported $Na_{2-2x}M_{1+x}P_2O_7$ (M = Mg, Ni) phases [20]. Currently, we are in the process of a detailed synchrotron structural analysis of this novel compound. From SEM analysis, the particle size was estimated to be 3–5 μm for solid-state synthesis and 300–500 nm for solution-combustion synthesis.

Though complex in nature, this structure offers large tunnels for Na-migration, thus offering a potential to be used as a cathode material. Mindful of the fact that the Na-based cathode materials are far less explored than their lithium counterparts and are mostly limited to oxides, the $Na_2FeP_2O_7$ can be a new member of a handful number of known polyanionic Na-cathode. Constituting naturally abundant Na, Fe and PO_4-species, it can be an economic cathode candidate for large scale sodium-ion batteries. In these contexts, we tested the electrochemical performance of solution-combustion prepared $Na_2FeP_2O_7$ cathode with no further cathode optimization such as carbon coating or particle down-sizing.

Upon the electrochemical cycling at a rate of C/20 (at 25 °C), a reversible capacity of 82 mAh·g^{-1} was obtained approaching one-

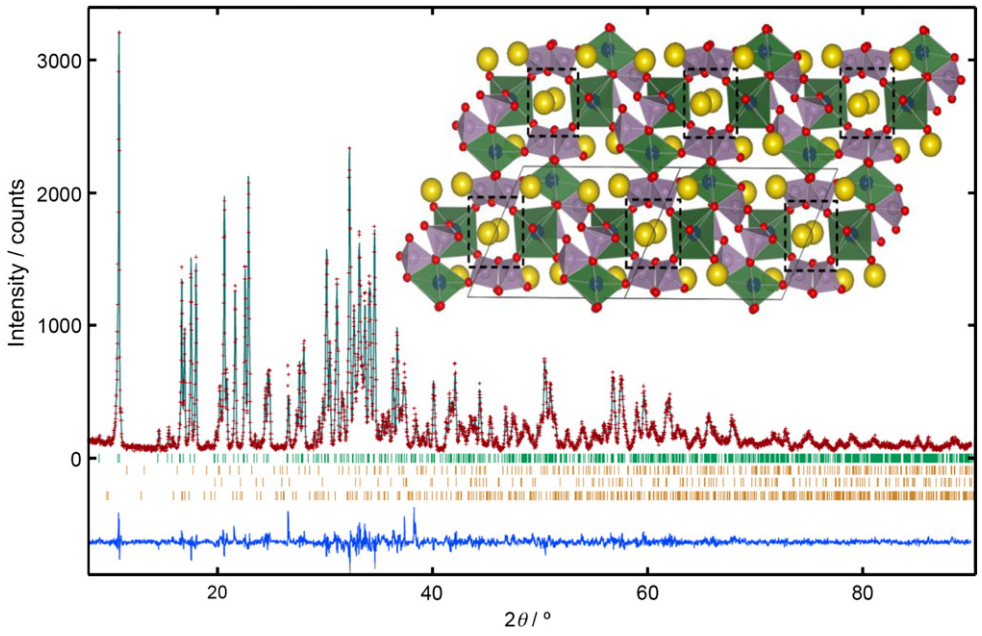

Fig. 1. X-ray diffraction with Rietveld refinement of $Na_2FeP_2O_7$ compound. The experimental data points (red dots), simulated powder pattern (green line), Bragg diffraction positions (green ticks for $Na_2FeP_2O_7$ and yellow ticks for impurities) and the difference between experimental and theoretical patterns (blue line) are shown. The product contains minimal $Na_4P_2O_7$ (7%), $NaFePO_4$ (1.5%) and $Na_4Fe_3(PO_4)_2(P_2O_7)$ (1.4%) impurity phases. (*Inset*) A representative illustration of the crystal structure viewed normal to the *bc* plane, showing tunnels favoring Na^+-ion migration as highlighted by black dotted rectangles. The FeO_6 octahedra (green), PO_4 tetrahedra (light purple) and Na atoms (yellow) are shown.

electron theoretical capacity of 97 mAh·g^{-1} (Fig. 2a). It involved a stair-case type voltage profile with a small plateau at 2.5 V followed by a large plateau at 3 V. Subsequent charge–discharge profiles were found to be neatly superimposing on each other resulting in an excellent capacity retention. As shown in the inset, the corresponding dQ/dV plot reveals the peak centered at 3 V consisting of three small steps (marked as 1, 2 and 3), which may signal a structural rearrangement or Na-ion ordering during Na (de)insertion reaction. This type of multi-step voltage–composition curve owing to the Na-ion/vacancy ordering has been observed in other Na-based cathodes such as P2-Na_xCoO_2 [21]. Afterwards, the rate capability was measured up to 10 C rate (Fig. 2b). Retaining the two characteristic plateaus at 2.5 V and 3.0 V, the $Na_2FeP_2O_7$ cathode showed excellent rate kinetics retaining 91% and 85% of the initial capacity at 1 C and 5 C rates respectively. This excellent kinetics can be attributed to the multi-dimensional open Na^+-ion diffusion channels and the presence of a ~5 nm surface carbon layer formed by the solution combustion process. The electrochemical performance of $Na_2FeP_2O_7$ cathode is quite promising, considering the fact that the solution-combustion prepared sample was relatively large (300–500 nm) with ~90% purity and was tested as such without any additional optimization. Further improvisation in synthesis and cathode formulation (e.g. particle nanosizing, carbon coating) can positively improve the electrochemical performance of this novel cathode.

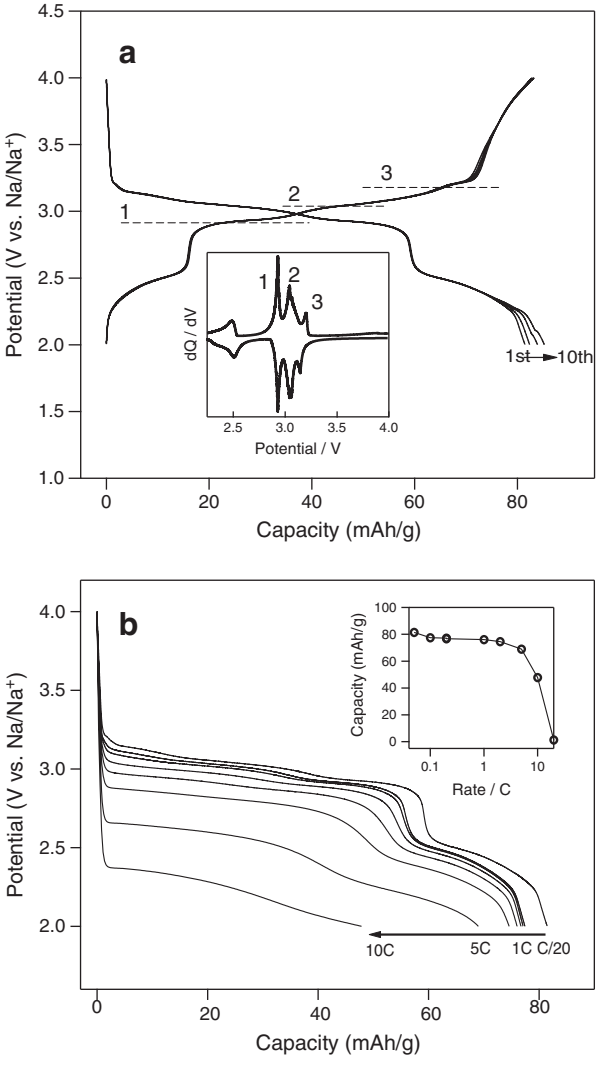

Fig. 2. Electrochemical characterization of $Na_2FeP_2O_7$. (a) Galvanostatic voltage–composition curve of $Na_2FeP_2O_7$ at a rate of C/20 (conducted at 25 °C) showing highly reversible Na (de)insertion activity with the average Fe^{3+}/Fe^{2+} redox potential centered at ~3 V. (*Inset*) The dQ/dV curve of charge–discharge profile showing several distinct peaks. The peak ~3 V has three distinct steps marked as 1, 2 and 3. (b) The discharge capacity of $Na_2FeP_2O_7$ as a function of rate is plotted to show the kinetics. (*Inset*) The capacity as a function of discharge rate is given. In each case, the cells were charged to 4 V at a constant rate of C/10 and were kept there for 1 h before discharging at different rates to 2 V.

The voltage–composition curves of $Na_2FeP_2O_7$ were found to be particularly atypical. To study the underlying Na (de)insertion reaction mechanism, $Na_2FeP_2O_7$ was chemically oxidized in an attempt to form $NaFeP_2O_7$. The XRD patterns and Mössbauer spectra of these $Na_{2-x}FeP_2O_7$ (x = 0–1) samples are shown in Fig. 3. Overall, the XRD patterns of $Na_{2-x}FeP_2O_7$ cathodes do not show any significant change involving approximately 2.1% volume shrinkage upon one Na removal, hinting at a topotactic Na (de)insertion reaction. The Mössbauer spectrum of pristine $Na_2FeP_2O_7$ shows mostly Fe^{2+}-species having two distinct iron sites, consistent with the crystal structure. Upon Na removal, the Fe^{2+} gradually converts into Fe^{3+} species involving continuous structural rearrangement. At present, the exact nature of electrochemical redox mechanism is not fully understood. We are undergoing a suite of electrochemical analysis to decipher this (de)insertion process.

4. Conclusions

In summary, we have reported a new Fe-based cathode, $Na_2FeP_2O_7$, for sodium ion batteries. Operating at an average voltage of 3 V (vs. Na/Na^+), it delivers a reversible capacity of 82 mAh·g^{-1} with a good rate capability. It is the first practical demonstration of a pyrophosphate class of cathode material for sodium-ion batteries. With its convenient synthesis, low cost, a theoretical capacity close to 100 mAh·g^{-1}, excellent reversibility and rate capability, $Na_2FeP_2O_7$ is a promising cathode material for future sodium-based batteries. It should encourage the battery community for further exploration of $Na_{2-x}MP_2O_7$ (M = Ti, Mn, Co, Ni, V) pyrophosphate phases as potential cathodes for Na-ion batteries. An in-depth study focusing on the underlying electrochemical reaction mechanism of optimized cathode will be presented in a future report.

Acknowledgments

The current research is financially supported by the Mitsubishi Motor Company. A part of this work was performed under a management of 'Element Strategy Initiative for Catalysts & Batteries' (ESICB) by the Ministry of Education, Culture, Sports, Science and Technology, Japan (MEXT). PB is grateful to the Japan Society for the Promotion of Sciences for a JSPS Fellowship and TY is grateful to Panasonic Inc. for a 'Panasonic Scholarship' at the University of Tokyo. The crystal structure was drawn using the VESTA software [22].

References

[1] V. Etacheri, R. Marom, R. Elazari, G. Salitra, D. Aurbach, Energy & Environmental Science 4 (2011) 3243.
[2] S.-W. Kim, D.-H. Seo, X. Ma, G. Ceder, K. Kang, Advanced Energy Materials 2 (2012) 710.
[3] C. Delmas, J.J. Braconnier, C. Fouassier, P. Hagenmuller, Solid State Ionics 4 (1981) 165.
[4] S. Komaba, C. Takei, T. Nakayama, A. Ogata, N. Yabuuchi, Electrochemistry Communications 12 (2010) 355.
[5] N. Yabuuchi, M. Kajiyama, J. Iwatate, H. Nishikawa, S. Hitomi, R. Okuyama, R. Usui, Y. Yamada, S. Komaba, Nature Materials 11 (2012) 512.
[6] P. Moreau, D. Guyomard, J. Gaubicher, F. Boucher, Chemistry of Materials 22 (2010) 4126.
[7] Z. Jian, L. Zhao, H. Pan, Y.-S. Hu, H. Li, W. Chen, L. Chen, Electrochemistry Communications 14 (2012) 86.
[8] J. Barker, M.Y. Saidi, J.L. Swoyer, Electrochemical and Solid-State Letters 6 (2003) 1.
[9] B.L. Ellis, W.R.M. Makahnouk, Y. Makimura, K. Toghill, L.F. Nazar, Nature Materials 6 (2007) 749.
[10] P. Barpanda, J.N. Chotard, N. Recham, C. Delacourt, M. Ati, L. Dupont, M. Armand, J.M. Tarascon, Inorganic Chemistry 49 (2010) 7401.
[11] S. Nishimura, M. Nakamura, R. Natsui, A. Yamada, Journal of the American Chemical Society 132 (2010) 13596.
[12] N. Furuta, S. Nishimura, P. Barpanda, A. Yamada, Chemistry of Materials 24 (2012) 1055.

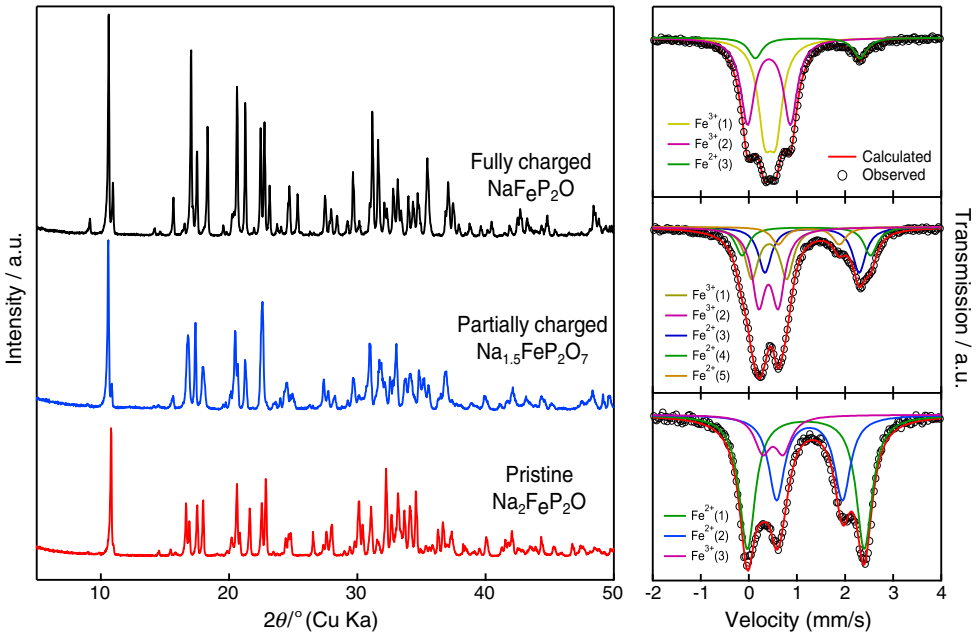

Fig. 3. XRD patterns and Mössbauer spectra of pristine and chemically oxidized $Na_{2-x}FeP_2O_7$ (x = 0–1) samples. For pristine $Na_2FeP_2O_7$, the Mössbauer spectra can be fitted with two Fe^{2+}-doublets (green and blue) indicating two crystallographically distinct Fe sites. The pink doublet shows Fe^{3+} impurities. Gradual desodiation increases the Fe^{3+} at the expense of Fe^{2+} species. The spectra of desodiated $NaFeP_2O_7$ can be fitted with two distinct Fe^{3+}-doublets (yellow and pink), with slight Fe^{2+} species (green).

[13] P. Barpanda, S. Nishimura, A. Yamada, Advanced Energy Materials 2 (2012) 841.
[14] H. Kim, I. Park, D.H. Seo, S. Lee, S.W. Kim, W.J. Kwon, Y.U. Park, C.S. Kim, S. Jeon, K. Kang, Journal of the American Chemical Society 134 (2012) 10369.
[15] P. Barpanda, T. Ye, S.C. Chung, Y. Yamada, S. Nishimura, A. Yamada, Journal of Materials Chemistry 22 (2012) 13455.
[16] A. Coelho, TOPAS-Academic Version 4.1 Computer Software, Coelho Software, Brisbane, Australia, 2007.
[17] http://www.mosswinn.com/english/index.html.
[18] F. Erragh, A. Boukhari, B. Elouadi, E.M. Holt, Journal of Crystallographic and Spectroscopic Research 21 (1991) 321.
[19] F. Sanz, C. Parada, J.M. Rojo, C. Ruiz Valero, R. Saez-Puche, Journal of Solid State Chemistry 145 (1999) 604.
[20] F. Erragh, A. Boukhari, F. Abraham, B. Elouadi, Journal of Solid State Chemistry 152 (2000) 323.
[21] D. Carlier, J.H. Cheng, R. Bertholet, M. Guignard, M. Yoncheva, R. Stoyanova, B.J. Hwang, C. Delmas, Dalton Transactions 40 (2011) 9306.
[22] K. Momma, F. Izumi, Journal of Applied Crystallography 44 (2011) 1272.